PAPER

Check for updates

Organic–inorganic hybrid metallic conductors based on bis(ethylenedithio)tetrathiafulvalene cations and antiferromagnetic oxalate-bridged copper(ii) dinuclear anions†

Bin Zhang, [ID] *[a] Yan Zhang,[b] Zheming Wang,*[c] Dongwei Wang,[d] Deliang Yang,[e] Zengqiang Gao,[f] Guangcai Chang,[f] Yanjun Guo,[d] Takehiko Mori, [ID] *[g] Zhijuan Zhao,[e] Fen Liu,[e] Qiaolian Li[e] and Daoben Zhu [ID] *[a]

The organic–inorganic hybrid β″-(BEDT-TTF)$_3$[Cu$_2$(μ–C$_2$O$_4$)(C$_2$O$_4$)$_2$(CH$_3$OH)(H$_2$O)] (BEDT-TTF = bis(ethylenedithio)tetrathia-fulvalene) composed of a BEDT-TTF donor and the oxalate-bridged binuclear anion [Cu$_2$(μ–C$_2$O$_4$)(C$_2$O$_4$)$_2$(CH$_3$OH)(H$_2$O)]$^{2-}$ has been obtained by electrocrystallization. It crystallizes in the triclinic $P\bar{1}$ space group with cell parameters of a = 7.4803(3) Å, b = 9.3547(3) Å, c = 18.6711(7) Å, $α$ = 95.797(3)°, $β$ = 90.974(3)°, $γ$ = 93.508(3)°, V = 1297.06(8) Å^3, and Z = 1 at 100 K. The donor arrangement belongs to the β″ phase. From the TTF core bond lengths and Raman spectroscopy, the oxidation state of BEDT-TTF is assigned to ∼ + 2/3. CH$_3$OH or H$_2$O molecules bond to the metal atoms at the apical position of the square pyramid with an occupancy of 0.5. A supramolecular square lattice forms through hydrogen bonds between the antiferromagnetic binuclear anions in the anion sheet. From the band structure at 100 K, metallic conductivity is expected, which agrees with four-probe conductivity measurements: its conductivity is 11.5 S cm^{-1} at room temperature, increases to 160 S cm^{-1} at 7.6 K, and then decreases to 150 S cm^{-1} at 2 K. From magnetic measurements, there is no long-range magnetic ordering, which is confirmed by specific heat measurements.

Introduction

Organic–inorganic hybrid charge-transfer salts composed of organic donors and inorganic magnetic anions provide many dual-functional molecular crystals showing magnetism, such as paramagnetism, long-range magnetic ordering, spin cross-over, and spin frustration, together with conductivity from insulating to semiconducting to metallic conductivity to even superconductivity. These materials have attracted considerable attention in materials science because of their potential uses in molecular spintronics and in the search for new superconductors.[1] The oxalate anion (C$_2$O$_4$$^{2-}$) is one of the most commonly used coordination ligands to mediate magnetic interactions between transition metals. Research on oxalate-bridged zero-dimensional (0D) binuclear compounds started in the 1970s and it is still active for molecular magnets.[2] Research has been extended to two-dimensional (2D) honeycomb metal-oxalate compounds, and the long-range ordered (LRO) [(C$_4$H$_9$)$_4$N][CrMn(μ–C$_2$O$_4$)$_3$] molecular ferromagnet and [(C$_4$H$_9$)$_4$N][Fe^{II}Fe^{III}(μ–C$_2$O$_4$)$_3$] molecular ferrimagnet were discovered in the 1990s.[3] Based on the oxalate-based molecular magnet with a honeycomb lattice, researchers have started to search for dual-functional molecular crystals composed of organic donors and inorganic metal-oxalate anions as charge-transfer salts. β″-(BEDT-TTF)$_4$[(H$_3$O)Fe(C$_2$O$_4$)$_3$]·C$_6$H$_5$CN (BEDT-TTF = bis(ethylenedithio)-tetrathiafulvalene), the first superconductor containing a magnetic atom, was reported in 1995.[4] The coexistence of ferromagnetic long-range order and metallic conductivity was observed in β-(BEDT-TTF)$_3$[CrMn(μ–C$_2$O$_4$)$_3$]·xCH$_2$Cl$_2$, and α-(BETS)$_3$[CrMn(μ–C$_2$O$_4$)$_3$]·

[a] *Organic Solid Laboratory, BNLMS, CMS & Institute of Chemistry, Chinese Academy of Sciences, Beijing, 100190, P. R. China. E-mail: zhangbin@iccas.ac.cn, zhudb@iccas.ac.cn*

[b] *Institute of Condensed Matter and Material Physics, Department of Physics, Peking University, Beijing, 100871, P. R. China*

[c] *State Key Laboratory of Rare Earth Materials Chemistry and Applications, BNLMS, College of Chemistry and Molecular Engineering, Peking University, Beijing, 100871, P. R. China. E-mail: zmw@pku.edu.cn*

[d] *CAS Key Laboratory of Standardization and Measurement for Nanotechnology, National Center for Nanoscience and Technology, Beijing, 100190, P. R. China*

[e] *CAS Research/Education Center for Excellence in Molecular Science, CMS & BNLMS, Institute of Chemistry, Chinese Academy of Sciences, Beijing, 100190, P. R. China*

[f] *BSRF, Institute of High Energy Physics, Chinese Academy of Sciences, Beijing, 100047, P. R. China*

[g] *Department of Materials Science and Engineering, Tokyo Institute of Technology, O-Okayama, Tokyo 152-8552, Japan. E-mail: mori_t_ae@m.titech.ac.jp*
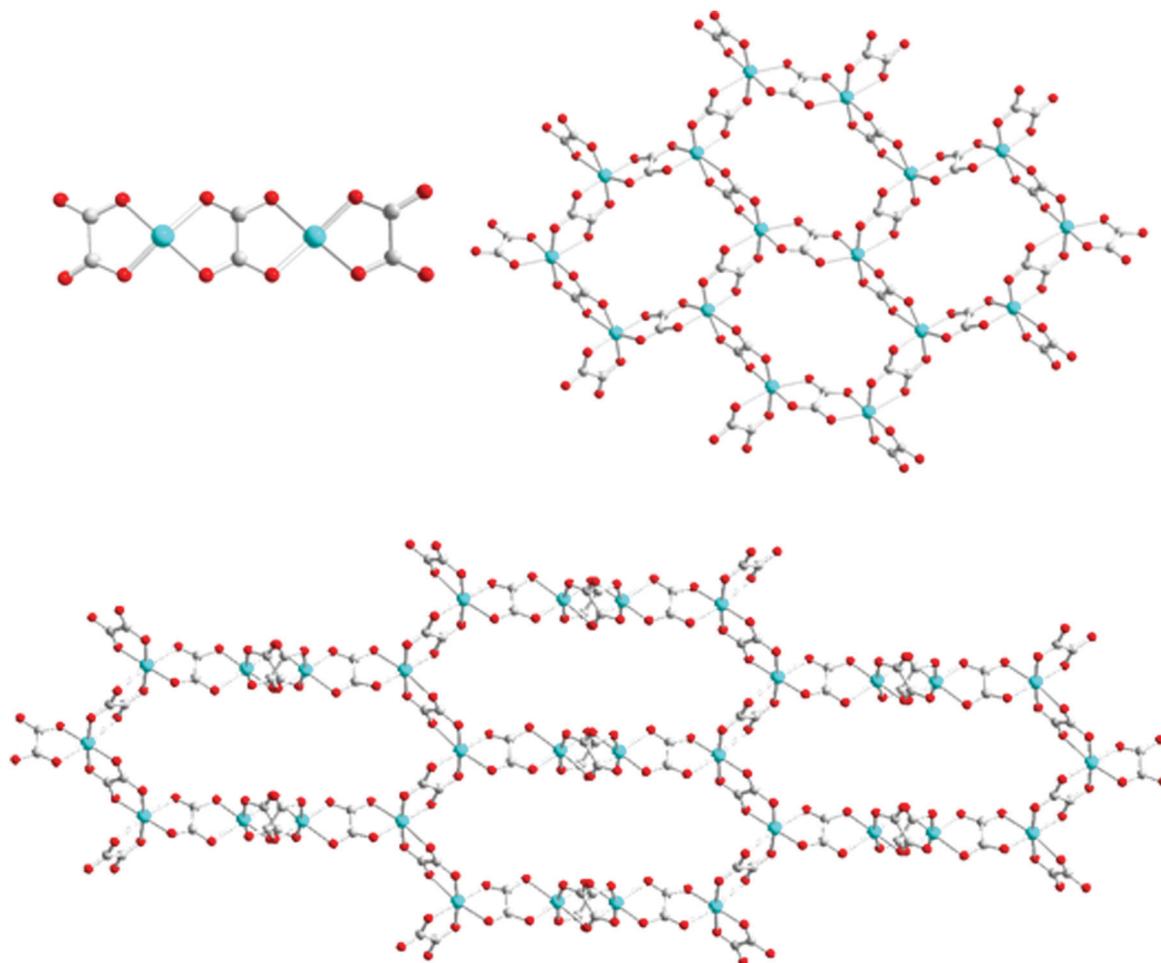
† Electronic supplementary information (ESI) available. CCDC 2019618, 2019619 and 2019620. For ESI and crystallographic data in CIF or other electronic format see DOI: 10.1039/d1tc04305f

This journal is © The Royal Society of Chemistry 2022

J. Mater. Chem. C, 2022, **10**, 2845–2852 | **2845**

xCH$_2$Cl$_2$ (BETS = bis(ethylenedithio)tetraselenafulvalene, x = 2–3) in the 2000s.[5] Strong antiferromagnetic behaviour without long-range ordering was observed in the θ^{21}-(BEDT-TTF)$_3$[Cu$_2$(μ–C$_2$O$_4$)$_3$]· 2CH$_3$OH (**2**) semiconductor and the θ^{21}-(BETS)$_3$[Cu$_2$(μ–C$_2$O$_4$)$_3$]· 2CH$_3$OH (**3**) conductor in the 2010s.[6] In organic–inorganic hybrid dual-functional molecular crystals with honeycomb metal-oxalate anions, organic molecules, such as C$_6$H$_5$CN, CH$_2$Cl$_2$, and CH$_3$OH, exist in the vacancies of the honeycomb lattice without bonding to the metal atoms.

The charge-transfer salts of 0D oxalate-bridged dinuclear anions, antiferromagnetic insulator TTF$_5$[Fe$_2$(μ–C$_2$O$_4$)(C$_2$O$_4$)$_4$] ·2C$_6$H$_5$CH$_3$· 2H$_2$O, antiferromagnetic semiconductor (BEDT-TTF)$_4$[Fe$_2$(μ–C$_2$O$_4$)(C$_2$O$_4$)$_4$] and TMTTF$_4$[Fe$_2$(μ–C$_2$O$_4$)(C$_2$O$_4$)$_4$]·C$_6$H$_5$CN·4H$_2$O, were reported in the 2000s.[7] They are different from the charge-transfer salts of 0D inorganic CuCl$_4^-$, FeCl$_4^-$ and FeBr$_4^-$ with the π-d interaction between the donor and anion from the S/Se···X interaction, such as the field-induced superconductivity in antiferromagnetic insulator λ-BETS$_2$FeCl$_4$, and the modulation of conductivity states between the insulator, metal, and superconductor by a magnetic field in λ-BETS$_2$Fe$_{0.4}$Ga$_{0.6}$Cl$_4$.[1,8]

In 0D oxalate-bridged dinuclear copper compounds, the interaction between the two Jahn–Teller distorted metal ions varies from ferromagnetic to antiferromagnetic.[9] Magnetostructural correlation plays an important role in compounds from classic molecular magnets to quantum spin liquids. For example, 0D oxalate-bridged [Cu$_2$(μ–C$_2$O$_4$)(C$_2$O$_4$)$_2$]$^{2-}$ is one of the coordination isomers of the 2D honeycomb [Cu$_2$(μ–C$_2$O$_4$)$_3$$^{2-}$]$_n$ and 3D hyperhoneycomb [Cu$_2$(μ–C$_2$O$_4$)$_3$$^{2-}$]$_n$ lattices (Scheme 1).[6,10] When the coordination environment of Cu^{2+} is modified from a square to an octahedron, 0D [Cu$_2$(μ–C$_2$O$_4$)(C$_2$O$_4$)$_2$]$^{2-}$ is the building block of the 2D honeycomb [Cu$_2$(μ–C$_2$O$_4$)$_3$$^{2-}$]$_n$ and 3D hyperhoneycomb [Cu$_2$(μ–C$_2$O$_4$)$_3$$^{2-}$]$_n$ lattices. The magnetic structures of the 3D hyperhoneycomb [Cu$_2$(μ–C$_2$O$_4$)$_3$$^{2-}$]$_n$ lattice obtained from Jahn–Teller distorted 0D Cu$_2$(μ–C$_2$O$_4$)(C$_2$O$_4$)$_4$$^{2-}$ orbital analysis show good agreement with theoretical analysis.[11,12] Spin frustration with $f > 10$ ($f = |\theta|/Tc$) has been observed in the molecular magnet and organic–inorganic hybrid dual-functional molecular crystals with the 2D honeycomb anions: insulating [(C$_3$H$_7$)$_3$NH]$_2$[Cu$_2$(μ–C$_2$O$_4$)$_3$]·2.2H$_2$O, semiconductive θ^{21}-(BEDT-TTF)$_3$[Cu$_2$(μ–C$_2$O$_4$)$_3$]·2CH$_3$OH, conductive θ^{21}-(BETS)$_3$[Cu$_2$(μ–C$_2$O$_4$)$_3$]·2CH$_3$OH, and insulating [(C$_2$H$_5$)$_3$NH]$_2$[Cu$_2$(μ–C$_2$O$_4$)$_3$]] with the 3D hyperhoneycomb anion.[6,12,13] [(C$_3$H$_7$)$_3$NH]$_2$[Cu$_2$(μ–C$_2$O$_4$)$_3$]·2.2H$_2$O has been suggested to be a candidate

Scheme 1 Three coordination isomers of [Cu$_2$(C$_2$O$_4$)$_3$$^{2-}$]: 0D (top left), 2D honeycomb (top right), and 3D hyperhoneycomb (bottom).

quantum spin liquid, and $[(C_2H_5)_3NH]_2[Cu_2(\mu-C_2O_4)_3)]$ has been confirmed to be a quantum spin liquid by μSR experiments.[10] When additional ligands bond to the coplanar 0D Cu_2 $(\mu-C_2O_4)(C_2O_4)_2^{2-}$ anions and the coordination mode of oxalate is maintained, it is possible to obtain a new magnetic network, even a 2D square lattice. Considering the magic magnetic properties of the 0D oxalate-bridged binuclear Cu anion and the Jahn–Teller effect, interesting conducting and magnetic properties are expected when the new anion is used as the counterion of charge-transfer salts as hole doping in La_2CuO_4.[14]

Herein, we report the organic–inorganic hybrid charge-transfer salt β''-(BEDT-TTF)$_3$[Cu$_2$(μ–C$_2$O$_4$)(C$_2$O$_4$)$_2$(CH$_3$OH)(H$_2$O)] composed of the BEDT-TTF donor and the binuclear oxalate-bridged Cu(II) anion.

Experimental

BEDT-TTF was obtained from commercial sources and used as received without further purification. C_6H_5Cl was dried over $CaCl_2$ and freshly distilled before use. CH_3OH was freshly distilled before use. $[C_2H_5)_3NH]_2[Cu_2(\mu-C_2O_4)_3]$ was obtained from a methanol solution of $Cu(NO_3)_2 \cdot 2H_2O$, $H_2C_2O_4 \cdot 2H_2O$, and Et_3N.[12] BEDT-TTF (5.0 mg) and $[(C_2H_5)_3NH]_2[Cu_2(\mu-C_2O_4)_3]$ (30.0 mg) were dissolved in a mixture of 25.0 mL distilled C_6H_5Cl, 5.0 mL distilled CH_3OH, and 0.3 mL distilled H_2O in an electrocrystallization cell at room temperature. After the colour of the solution became transparent orange, the cell was subjected to a constant current of 0.17 μA. A shiny yellow-green thin-plate crystal was obtained on the anode after one month (Fig. S1, ESI†).

A single crystal with dimensions of 0.112 mm × 0.076 mm × 0.061 mm was selected for the X-ray diffraction experiment using a Rigaku Oxford diffractometer with Mo K$_\alpha$ radiation (λ = 0.71073 Å). The diffraction data were collected at 290, 180, and 100 K. The data were reduced with CrysAlisPro.[15] The crystal structure was solved by the direct method with SHELX86 and refined by the full-matrix method with SHELX2014.[16] The crystallographic data are given in Table S1 (ESI†). The H_2O or CH_3OH terminal ligand bonded to Cu by a Cu–O bond. The position of the H atom of the O–H group shared by H_2O and CH_3OH was determined from the difference Fourier map and refined by constraints. The C atom of methanol was determined from the difference Fourier map and refined anisotropically. The H atoms of the CH_3 group of CH_3OH and CH_2 group of the donor were assigned by calculations and refined isotropically. The O–H distance in H_2O was fixed during refinement. The refined occupation of the C atom of methanol was ~0.50, so the terminal ligand bonds to Cu was composed of $(H_2O)_{0.5}(CH_3OH)_{0.5}$. This corresponds to the elemental analysis (%): calcd for $C_{37}H_{30}Cu_2O_{14}S_{24}$ (1595): C 27.86, H 1.90. Found: C 27.63, H 1.85.

Several single crystals were selected for Raman spectroscopy. Raman spectroscopy was performed with a Renishaw inVia Raman microscope at room temperature using λ = 514.5 nm.

The conductivity measurements were performed by the four-probe method with 13 μm gold wires attached by gold paste on the best developed surface of a single crystal from 2 to 300 K using a Quantum Design PPMS 9XL system.

The magnetization measurements were performed for crystals tightly packed in an Al bag using a Quantum Design MPMS 7XL system. The data were corrected by the background, and the Pascal constant (-352.2×10^{-6} cm^3 mol^{-1} per Cu^{2+}).[17]

Results and discussion

When the $[(C_2H_5)_3NH]_2[Cu_2(\mu-C_2O_4)_3]$ 3D hyperhoneycomb ammonium salt was used as the starting material together with H_2O present in the distilled solution of C_6H_5Cl and CH_3OH, the $[Cu_2(\mu-C_2O_4)_3^{2-}]_n$ 3D hyperhoneycomb decomposed to the 0D $Cu_2(\mu-C_2O_4)(C_2O_4)_2^{2-}$ oxalate-bridged binuclear unit, and H_2O and CH_3OH from the solvent bonded to the metal atom by Cu–O bonds to give β''-(BEDT-TTF)$_3$[Cu$_2$(μ–C$_2$O$_4$)(C$_2$O$_4$)$_2$ (CH$_3$OH)(H$_2$O)] (**1**). In an anhydrous solution of C_6H_5Cl and CH_3OH, the 3D $[Cu_2(\mu-C_2O_4)_3^{2-}]_n$ hyperhoneycomb lattice changed to the 2D $[Cu_2(\mu-C_2O_4)_3^{2-}]_n$ honeycomb lattice. CH_3OH was incorporated into the cavity of the honeycomb lattice, and θ^{21}-(BEDT-TTF)$_3$[Cu$_2$(μ–C$_2$O$_4$)$_3$]·2CH$_3$OH (**2**) was obtained.[6] The difference in crystal growth between **1** and **2** originates from the presence of H_2O in the solution. Thus, **1** and **2** can be controllably synthesized.

The single-crystal structure of **1** remained the same from 100 K to 290 K and the data at 100 K were used for structural discussion. At 100 K, it crystallizes in the $P\bar{1}$ space group with cell parameters of a = 7.4803(3) Å, b = 9.3547(3) Å, c = 18.6711(7) Å, α = 95.797(3)°, β = 90.974(3)°, γ = 93.508(3)°, V = 1297.06(8) Å^3, and Z = 1. There are one (A) and a half (B) donor molecules, half of an anion composed of one Cu, one and half $C_2O_4^{2-}$ ions, half a H_2O molecule, and half a CH_3OH molecule in an independent unit (Fig. 1). Accordingly, a unit cell contains three BEDT-TTF molecules and one oxalate-bridged binuclear anion $[Cu_2(\mu-C_2O_4)(C_2O_4)_2(CH_3OH)(H_2O)^{2-}]$.

1 consists of three donor molecules, two Cu atoms, three oxalate anions, and two neutral molecules, which is the same as that reported for **2** and θ^{21}-(BETS)$_3$[Cu$_2$(μ–C$_2$O$_4$)$_3$]·2CH$_3$OH,[6] **2** and θ^{21}-(BETS)$_3$[Cu$_2$(μ–C$_2$O$_4$)$_3$]·2CH$_3$OH are isostructural
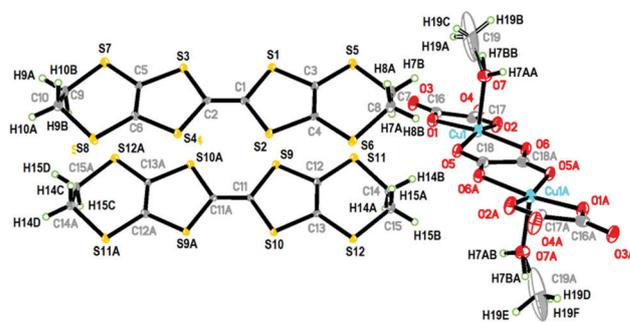

Fig. 1 Atomic structure of **1** in an independent unit with 50% ellipsoids. The occupations of H7BB, C19, H19A, H19B, H7BA, C19A, H19C, H19D, H19E, and H19F are 50%. Asymmetry code A: 1−x, 1−y, −z.

This journal is © The Royal Society of Chemistry 2022

J. Mater. Chem. C, 2022, **10**, 2845–2852 | **2847**

compounds. However, the crystal structures of **1** and **2** are different. Comparing the cell volumes of **1** and **2** at 290 K, the 200 Å^3 difference is more than the volume of two CH_3 groups. This means that there is tight packing of the organic and inorganic building blocks inside the **1** crystal.

In **1**, the donor molecules stack in a quasi-face-to-face mode along the [−110] direction with the sequence of −A–A–B− (Fig. 2b). Although the stack is composed of a trimer unit, there is no displacement, and the stack is practically uniform. The in-plane displacement between the neighbouring donor molecules is almost half a molecule along the b axis. There are C–H···S interactions between the donor molecules.

The donor columns are arranged side-by-side along the [1–10] direction, where there are S···S contacts and C–H···S interactions between the columns. The donor arrangement belongs to the β'' phase, as observed in the organic superconductors β''-(BEDT-TTF)$_2$I$_3$, and β''-(BEDT-TTF)$_4$[(H$_3$O)Fe(C$_2$O$_4$)$_3$]·C$_6$H$_5$CN.[4,18] This is different from **2** and θ^{21}-(BETS)$_3$[Cu$_2$(µ–C$_2$O$_4$)$_3$]·2CH$_3$OH, where the donor arrangement belongs to the θ^{21} phase (Fig. S3, ESI†).[6] Considering the bond length of the TTF core with the standard deviation of 0.1 of δ, the oxidation state of BEDT-TTF is in basic agreement with the +2/3 average charge (Table 1), and it remained the same at 180 and 290 K (Table S2, ESI†).[19]

The C=C stretching frequency of the charge-transfer complexes of BEDT-TTF is a powerful way to determine the oxidation state. In the Raman spectrum of **1** (Fig. 3), the ν_2 mode is observed at 1488 cm^{-1}. This is the same as that of charge-transfer salts with BEDT-TTF$^{+2/3}$. The formal charge is deduced to be 0.66.[20]

The [Cu$_2$(µ–C$_2$O$_4$)(C$_2$O$_4$)$_2$(CH$_3$OH)(H$_2$O)$^{2-}$] anion is a 0D oxalate-bridged binuclear anion (Fig. 2c). The oxalate-bridged 0D Cu$_2$(µ–C$_2$O$_4$)(C$_2$O$_4$)$_2$$^{2-}$ unit is one of the coordination isomers of [Cu$_2$(µ–C$_2$O$_4$)$_3$$^{2-}$], which have been reported to have 2D honeycomb and 3D hyperhoneycomb lattices (Scheme 1). In the anion, the Cu^{2+} atoms are square-pyramidally coordinated to two O atoms from the bisbidentate oxalate anion and two O atoms from the bidentate oxalate anion in the basal plane, and the O atom from H$_2$O or CH$_3$OH from the apical position. It is different from the 0D oxalate-bridged dinuclear anion [Fe$_2$(µ–C$_2$O$_4$)(C$_2$O$_4$)$_4$$^{4-}$], and the Fe^{3+} atoms are octahedrally coordinated with two O atoms from the bisbidentate oxalate anions and four O atoms from the bidentate oxalate anions.[7] In the basal plane, the Cu–O distances are 1.930(4)–2.001(3) Å. The metal atoms lie in the main plane of the bidentate oxalate anion. The planes of the two bidentate oxalate anions are staggered from the plane of the bisbidentate oxalate anion with an angle of 10.3(2)° in a "chair" conformation. The Cu–O distance from Cu to CH$_3$OH and H$_2$O is 2.231(4) Å. There are O–H···O hydrogen bonds between the anions, from H$_2$O/CH$_3$OH to uncoordinated O atoms on the bidentate oxalate anion (Fig. 2c). Because the methanol CH$_3$ group is oriented outside of the anion with occupation of 0.5, the occupation of the inside H atom is 1.0, and the occupation of another H atom of H$_2$O with the same orientation as the CH$_3$ group is 0.5. The hydrogen bond between the oxalate anion and apical ligand is along the a axis, as shown by thick dashed blue lines in Fig. 2c.
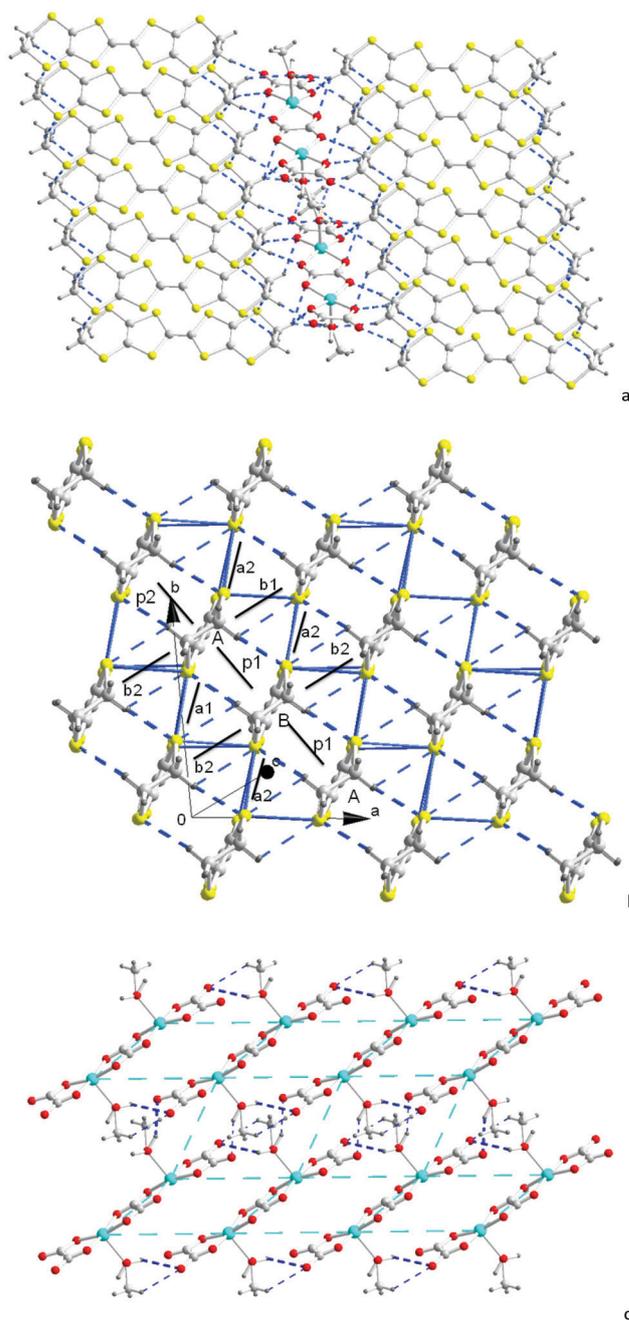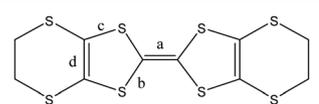

Fig. 2 Crystal structure of **1**: (a) packing diagram viewed along the a axis, (b) donor arrangement viewed along the c axis with the definition of the overlap integrals, and (c) anion arrangement viewed along the c axis. Colour code: Cu, cyan; O, red; S, yellow; C, grey; H, dark grey; hydrogen bonds, blue dash lines; S···S contacts, blue solid lines. The dashed cyan lines show the hydrogen-bonded 4 × 4 grid. The transfer integrals (black solid lines) are: p1, −43.8; p2, −29.8; a1, 175.8; a2, 176.4; b1, −82.8; b2, −96.1 meV.

The disordered hydrogen bonds in the anion sheet form a supramolecular square lattice of metal atoms. The Cu···Cu distances are 5.215 Å within the binuclear anion, and 6.690 and 7.480 Å between the Cu atoms connected through an O–H···O hydrogen bond. When the temperature is decreased from 300
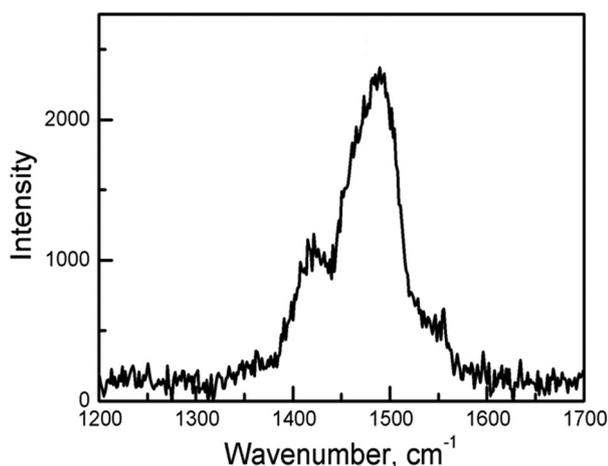
Table 1 Formal charges of the BEDT-TTF molecules at 100 K

$\delta = (b+c)-(a+d)$

$Q = 6.347 - 7.463\delta$

	a	B	c	d	δ	Q
A	1.368	1.733	1.750	1.355	0.756	0.705
		1.735	1.748	1.358		
		1.733	1.746			
		1.731	1.746			
B	1.372	1.730	1.744	1.359	0.745	0.787
		1.730	1.748			
Total						2.2

Fig. 3 Raman spectra of the best developed surfaces of single crystals of **1** with λ = 514.5 nm at room temperature.

Table 2 C–H···O hydrogen bonds between the donor and anion

D–H···A	H···A, Å	D···A, Å	∠ D–H···A,°
C7–H7A···O	2.66	3.333(5)	125.6
C8–H8B···O5	2.65	3.311(5)	124
C9–H9A···O3	2.38	3.241(5)	145.7
C10–H10A···O2	2.54	3.234(5)	127.2
C10–H10A···O6	2.57	3.333(5)	133.6
C14–H14B···O1	2.43	3.218(5)	136.6
C15–H15B···O4	2.40	3.388(5)	172.8

Fig. 4 Temperature dependence of the conductivity of **1**. The inset shows the resistance in the low-temperature range.

to 100 K, the Cu–O distances on the square plane elongate, the apical Cu–O distance contracts, and the Jahn–Teller distortion remains.

There are C–H···O hydrogen bonds between the donor and the anion (Table 2). The S···X and Se···X contacts between the donor and anion, which are observed in charge-transfer salts composed of an organic donor and inorganic anion 0D mononuclear $CuCl_4^{2-}$, $FeCl_4^-$, $FeBr_4^-$, dinuclear $[Cu_2(\mu–Cl)_2Cl_4^{2-}]$ and 1D $[Fe(\mu–C_2O_4)Cl_2^-]_n$, do not exist.[1,8,21]

The room-temperature conductivity of **1** is 11.5 S cm^{-1}. When the temperature decreases, the conductivity increases, similar to that of a metal, and reaches 160 S cm^{-1} at 7.6 K, and it then slowly decreases to 150 S cm^{-1} at 2 K (Fig. 4). This is different from charge-transfer salts with the same donor arrangement: β''-(BEDT-TTF)$_3$(HSO$_4$)$_2$, β''-(BEDT-TTF)$_3$(ReO$_4$)$_2$, and β''-(BEDT-TTF)$_3$(ClO$_4$)$_2$, which show a metal–insulator transition at around 150, 100, and 170 K, respectively, accompanied by charge ordering.[22] This is different from the reported charge-transfer salts of 0D oxalate-bridged iron dinuclear anions, insulator TTF$_5$[Fe$_2$(μ–C$_2$O$_4$)(C$_2$O$_4$)$_4$]·2C$_6$H$_5$CH$_3$·2H$_2$O,

semiconductor (BEDT-TTF)$_4$[Fe$_2$(μ–C$_2$O$_4$)(C$_2$O$_4$)$_4$] and TMTTF$_4$[Fe$_2$(μ–C$_2$O$_4$)(C$_2$O$_4$)$_4$], and C$_6$H$_5$CN·4H$_2$O and 2D oxalate-bridged anions, semiconductor **2** and conductor θ^{21}-(BETS)$_3$[Cu$_2$(μ–C$_2$O$_4$)$_3$]·2CH$_3$OH with a metal-semiconductor transition at 150 K.[6]

To understand the conductivity behaviour, the electronic structure was analyzed. Because there are no strong interactions between the donor and anion as observed in λ-(BETS)$_2$FeCl$_4$, κ-BETS$_2$FeBr$_4$ and TTF$_2$Fe(μ–C$_2$O$_4$)Cl$_2$, we can ignore the π–d interaction.[1,21] The electronic structure of **1** is determined by the organic donor layer, similar to β-(BEDT-TTF)$_3$[CrMn(μ–C$_2$O$_4$)$_3$]·xCH$_2$Cl$_2$, **2** and θ^{21}-(BETS)$_3$[Cu$_2$(μ–C$_2$O$_4$)$_3$]·2CH$_3$OH.[5,6] The band structure was calculated from the transfer integrals between the donor molecules using the tight-binding approach (Fig. 2b).[23] The resulting band structure shows strong dispersion (Fig. 5). The Fermi surface consists of a hole pocket around the Y point and an electron pocket around the Γ point, but the global feature is derived from a large elliptical surface associated with the very small trimerization. This energy band agrees with the metallic conductivity, as expected from the conductivity measurements above 7.6 K.

In charge-transfer salts with metal-oxalate anions, the magnetic property is always controlled by the inorganic anion, and it varies from paramagnetic 0D Fe(C$_2$O$_4$)$_3$$^{3-}$, antiferromagnetic 0D [Fe$_2$(μ–C$_2$O$_4$)(C$_2$O$_4$)$_4$$^{4-}$], and antiferromagnetic LRO for 1D [Fe(μ–C$_2$O$_4$)Cl$_2$$^-$]$_n$ to ferromagnetic LRO for 2D [CrMn
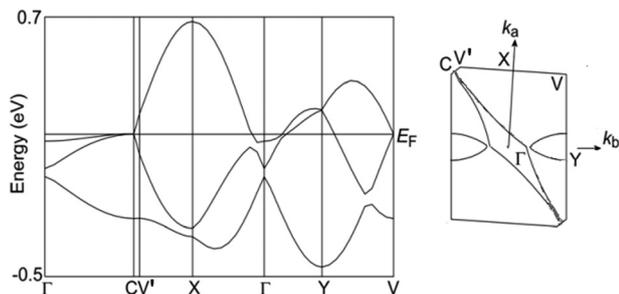
Fig. 5 Band structure and Fermi surface of **1**.

$(\mu–C_2O_4)_3]^-_n$ to spin frustration for 2D $[Cu_2(\mu–C_2O_4)_3^{2-}]_n$.[4–7,21] By empirical orbital analysis, the interaction between the Cu spins within the dinuclear anions can be analyzed.[9] The magnetic orbital $(d_{x^2-y^2})$ on two metal atoms is coplanar, so a strong antiferromagnetic interaction is expected. The temperature-dependent susceptibility was measured under 10 000 Oe. The Pauli paramagnetism from the conducting unit in **1** should be in the same range as observed in charge-transfer complexes with ET_2^{3+}. For example, in organic conductors β''-(BEDT-TTF)$_3$(ClO$_4$)$_2$ and β''-(BEDT-TTF)$_3$(HSO$_4$)$_2$, the Pauli paramagnetism is $6.5–7.5 \times 10^{-4}$ cm^3 mol^{-1}.[24] At 300 K, χT is 0.408 cm^3 K mol^{-1} after Pauli paramagnetism was subtracted (Fig. 6). It is similar to the previously reported value in honeycomb copper-oxalate-framework compounds with Jahn–Teller distortion at 300 K [**2**, 0.43 cm^3 K mol^{-1}; [(C$_3$H$_7$)$_3$NH]$_2$[Cu$_2$(μ–C$_2$O$_4$)$_3$]·2.2H$_2$O, 0.465 cm^3 K mol^{-1}], and a square copper-format-framework compound at 300 K [θ-(BEDT-TTF)$_2$Cu$_2$(μ–HCOO)$_5$, 0.494 cm^3 K mol^{-1}].[6,11,25]

With a decreasing temperature, the χ value smoothly increases with a broad shoulder at around 190 K. Below 190 K, it decreases and reaches a minimum at 55 K. The χ value then increases and reaches 0.008 cm^3 mol^{-1} at 2 K. From the broad maximum around 190 K, it is an antiferromagnetic system, and the antiferromagnetic interaction J could be estimated from the empirical function $|J|/kT_{max} = 1.599$ as -304 K.

The temperature dependent susceptibility data were analyzed by a "singlet–triplet" model with $H = -JS_A \cdot S_B$, with
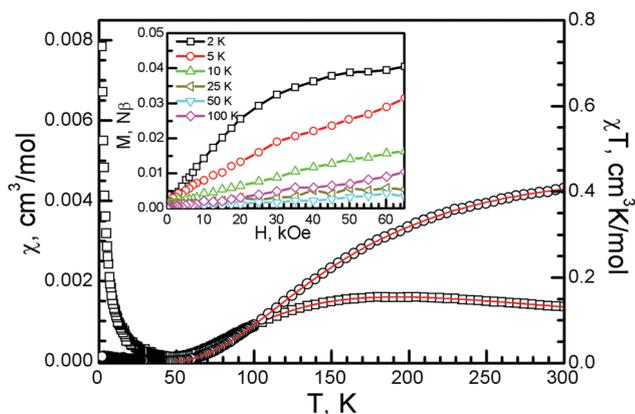

Fig. 6 Temperature dependence of the magnetic susceptibility, χ (squares) and χT (circles), together with the dimer model (red lines). The inset shows the isothermal magnetization at 2, 5, 10, 50 and 100 K.

intermolecular interaction between dinuclear units, which was used for oxalate-bridged copper dinuclear compounds.[26] The equation was used to fit the results above 50 K, giving $g = 2.01$ (1), $J = -323(1)$ K, and $R = 1.56 \times 10^{-7}$ ($R = \Sigma(\chi_0-\chi_c)^2/\Sigma\chi_0^2$). This shows that the singlet–triplet energy gap of **1** is above 200 cm^{-1}, which is in the same range as that of the reported oxalate-bridged dinuclear Cu(ɪɪ) compounds.[26]

The isothermal magnetization was measured at temperatures from 2 to 300 K (Fig. 6, inset). The isothermal magnetization smoothly increased and reached 0.0395 Nβ at 65 kOe and 2 K, which is much smaller than the value of 1 Nβ for isolated, spin only Cu^{2+} with $S = 1/2$ and $g = 2.0$. The magnetization linearly increased with increasing magnetic field and reached 0.0033 Nβ at 50 K and 0.0104 Nβ at 100 K. These values confirm the strong antiferromagnetic interaction between the oxalate-bridged metal atoms. They are in the same range as those of the 3D hyperhoneycomb compound [(C$_2$H$_5$)$_3$NH]$_2$[Cu$_2$(μ–C$_2$O$_4$)$_3$] (0.0351 Nβ at 2 K, 0.0304 Nβ at 5 K, and 0.0145 Nβ at 300 K and 65 kOe) and the 2D honeycomb compound [(C$_3$H$_7$)$_3$NH]$_2$[Cu(μ–C$_2$O$_4$)$_3$]·2.2H$_2$O (0.044 Nβ at 2 K and 65 kOe).[12] They are also comparable with those of the oxalate-bridged binuclear copper compound {[tmen(2-MeIm)Cu]$_2$(C$_2$O$_4$)}(PF$_6$)$_2$, for which the isothermal magnetization has been estimated to be about 0.05 Nβ at 70 kOe.[27] Zero-field-cooled, field-cooled, and remnant magnetization measurements from 2 to 100 K under 100 Oe showed no bifurcation (Fig. S3, ESI†).

Specific heat experiments were performed from 2 to 120 K under 0 and 5 T (Fig. S4, ESI†). No λ-peak was observed between 2 and 120 K. Combining with the X-ray diffraction experiment from room temperature to 100 K, there is neither magnetic ordering nor a structural transition between 2 and 290 K.

Because the susceptibility measurements were performed with selected high-quality crystals, the antiferromagnetic interaction should be the intrinsic behaviour of the crystal. The observed magnetic properties are determined not only by the oxalate-bridged binuclear anion, but also by the hydrogen-bonded square lattice anion. Because the magnetic interaction through hydrogen bonds is around 1–10 cm^{-1} and much weaker than the oxalate-bridge, the magnetic interactions between the anions should be much weaker than the intradimer interaction.[27] The magnetic properties of **1** are controlled by the oxalate-bridged binuclear anion sheet.

Conclusions

β''-(BEDT-TTF)$_3$[Cu$_2$(μ–C$_2$O$_4$)(C$_2$O$_4$)$_2$(CH$_3$OH)(H$_2$O)] is the first magnetic organic conductor incorporating oxalate-bridged binuclear Cu(ɪɪ) anions. It shows metallic conductivity down to 2 K and proves that modification of the donor arrangement improves the conductivity from its polymorphic compound θ^{21}-(BEDT-TTF)$_3$[Cu$_2$(μ–C$_2$O$_4$)$_3$]·2 solvent rather than by replacement of S by Se on the TTF core to obtain the isostructural compound θ^{21}-(BETS)$_3$[Cu$_2$(μ–C$_2$O$_4$)$_3$]·2 solvent. The antiferromagnetic interaction in the hydrogen-bonded oxalate-bridged

2850 | *J. Mater. Chem. C*, 2022, **10**, 2845–2852

This journal is © The Royal Society of Chemistry 2022

Cu(II) binuclear anion square lattice is stronger than that in the $[Cu_2(\mu-C_2O_4)_3{}^{2-}]_n$ honeycomb lattice. No long range order is observed above 2 K. β''-(BEDT-TTF)$_3$[Cu$_2$(μ-C$_2$O$_4$)(C$_2$O$_4$)$_2$(CH$_3$OH)(H$_2$O)] is a new member of magnetic conductors.

Author contributions

The manuscript was written through contributions from all authors. B. Zhang and D. Zhu managed the project. B. Zhang and Y. Zhang synthesised the samples. Y. Zhang performed magnetic measurements. Z. Wang, Z. Gao and G. Chang carried out single crystal X-ray diffraction experiments. Y. Zhang and D. Wang carried out conductivity and heat capacity experiments. D. Yang performed the EDS measurements. G. Yan recorded the Raman spectra. Z. Zhao and F. Liu carried out XPS experiments. T. Mori carried out ESR experiments and calculated the band structure. Q. Li carried out elemental analysis experiments. B. Zhang conducted experiments and analyzed the data. B. Zhang, T. Mori, Y. Zhang and Z. Wang wrote the main manuscript text. All authors have given approval to the final version of the manuscript.

Abbreviations

BEDT-TTF   bis(ethylenedithio)tetrathiafulvalene.
BETS   bisethylene(tetraselenafulvalene).

Conflicts of interest

There are no conflicts to declare.

Acknowledgements

Notes and references

1 P. Day, M. Kurmoo, T. Mallah, I. Marsden, R. Friend, F. Pratt, W. Hayes, D. Chasseau, J. Gaultier, G. Bravis and L. Ducasse, *J. Am. Chem. Soc.*, 1992, **114**, 10722; P. Cassoux, *Science*, 1997, **272**, 1277; H. Kobayashi, H. Tomita, T. Naito, A. Kobayashi, F. Sakai, T. Watanabe and P. Cassoux, *J. Am. Chem. Soc.*, 1996, **118**, 368; F. Palacio and J. S. Miller, *Nature*, 2000, **408**, 421; H. Kobayashi, H. Cui and A. Kobayashi, *Chem. Rev.*, 2004, **104**, 5265.

2 T. R. Felthouse, E. J. Laskowski and D. N. Hendrickson, *Inorg. Chem.*, 1977, **16**, 1077; M. Julve, M. Verdaguer, A. Gleizes, M. Philoche-Levisalles and O. Kahn, *Inorg. Chem.*,

1984, **23**, 3808; O. Kahn, *Angew. Chem., Int. Ed. Engl.*, 1985, **24**, 834; M. Julve, A. Gleizes, L. M. Chamoreau, E. Ruiz and M. Verdaguer, *Eur. J. Inorg. Chem.*, 2018, 509 and references cited therein.

3 H. Tamaki, Z. J. Zhong, N. Matsumoto, S. Kida, M. Koikawa, N. Achiwa, Y. Hashimoto and H. Okawa, *J. Am. Chem. Soc.*, 1992, **114**, 6974; C. Mathoniere, S. G. Carling, D. Yusheng and P. Day, *J. Chem. Soc., Chem. Commun.*, 1994, 1551.

4 A. W. Graham, M. Kurmoo and P. Day, *J. Chem. Soc., Chem. Commun.*, 1995, 2061; P. Cassoux, *Science*, 1997, **272**, 1277; S. Benmansour and C. J. Gomez-Garcia, *Magnetochemistry*, 2021, **7**, 93.

5 E. Coronado, J. R. Galan-Mascaros, C. J. Gomez-Garcia and V. Laukhin, *Nature*, 2000, **408**, 447; A. Albertola, E. Coronado, J. R. Galan-Mascaros, C. Gimenez-Saiz and C. J. Gomez-Garcia, *J. Am. Chem. Soc.*, 2003, **125**, 10774.

6 B. Zhang, Y. Zhang and D. Zhu, *Chem. Commun.*, 2012, **48**, 197; B. Zhang, Y. Zhang, Z. Wang, S. Gao, Y. Guo, F. Liu and D. Zhu, *CrystEngComm*, 2013, **15**, 3529.

7 M. Clemente-Leon, E. Coronado, J. Galan-Mascaros, C. Gimenez-Saiz, C. Gomez-Garcia and J. Fabre, *Synth. Met.*, 1999, **103**, 2279; S. Rashid, S. Turner, P. Day, M. Light and M. Hursthouse, *Inorg. Chem.*, 2000, **39**, 2426; E. Coronado, J. Galan-Mascaros and C. Gomez-Gracia, *J. Chem. Soc., Dalton Trans.*, 2000, **2**, 205.

8 P. Day, M. Kurmoo, T. Mallah, I. Marsden, R. Friend, F. Pratt, W. Hayes, D. Chasseau, J. Gaultier, G. Bravic and L. Ducasse, *J. Am. Chem. Soc.*, 1992, **114**, 10772; H. Kujiwara, E. Fujiwara, Y. Nakazawa, B. Narymbetov, K. Kato, H. Kobayashi, A. Kobayashi, M. Tokumoto and P. Cassoux, *J. Am. Chem. Soc.*, 2001, **123**, 306; B. Zhang, H. Tanaka, H. Fujiwara, H. Kobayashi, E. Fujiwara and A. Kobayashi, *J. Am. Chem. Soc.*, 2002, **124**, 9982.

9 O. Kahn, *Angew. Chem.*, 1985, **24**, 834; O. Kahn, O. Kahn, *Molecular Magnetism*, VCH Publisher, Inc., 1993, p. 103; J. Cano, P. Alemany, S. Alvarez, M. Verdaguer and E. Ruiz, *Chem. – Eur. J.*, 1998, **4**, 476.

10 B. Zhang, Y. Zhang, Z. Wang, D. Wang, P. Baker, F. Pratt and D. Zhu, *Sci. Rep.*, 2014, **4**, 06451; B. Zhang, P. Baker, Y. Zhang, D. Wang, Z. Wang, S. Su, D. Zhu and F. Pratt, *J. Am. Chem. Soc.*, 2018, **140**, 122.

11 A. C. Jacko and B. J. Powell, *arXiv*: 1805.05495.

12 B. Zhang, Y. Zhang and D. Zhu, *Dalton Trans.*, 2012, **14**, 8509.

13 L. Balents, *Nature*, 2010, **464**, 199.

14 P. W. Anderson, *Science*, 1987, **235**, 1196.

15 *CrysAlisPro 1.171.39.9f*, Rigaku OD, 2015.

16 G. M. Sheldrick, *SHELX97*, University of Göttingen, Göttingen, Germany, 1997; G. M. Sheldrick, *SHELXL-2014/7*, University of Göttingen, Göttingen, Germany, 2014.

17 O. Kahn, *Molecular Magnetism*, VCH Publisher, Inc., 1993, p. 3.

18 T. Mori, *Bull. Chem. Soc. Jpn.*, 1998, **71**, 2509; T. Mori, *Electronic Properties of Organic Conductors*, Springer, 2016.

19 P. Guionneau, C. J. Kepert, G. Bravis, D. Chasseau, M. R. Truter, M. Kurmoo and P. Day, *Syn. Met.*, 1997, **86**, 1973.

20 H. H. Wang, J. R. Ferraro, J. M. Williams, U. Geiser and J. A. Schlueter, *J. Chem. Soc., Chem. Comm.*, 1994, 1893; T. Yamamoto, M. Uruichi, K. Yamamoto, K. Yakushi, A. Kawamoto and H. Taniguchi, *J. Phys. Chem. B.*, 2005, **109**, 15226.

21 A. Kobayshi, A. Sato, A. Arai, H. Kobayashi, C. Faulmann, N. Kushch and P. Cassoux, *Solid State Commun.*, 1997, **103**, 371; B. Zhang, Z. Wang, H. Fujiwara, H. Kobayashi, M. Kurmoo, K. Inoue, T. Mori, S. Gao, Y. Zhang and D. Zhu, *Adv. Mater.*, 2005, **17**, 1988; B. Zhang, Z. Wang, Y. Zhang, K. Takahashi, Y. Okano, H. B. Cui, H. Kobayashi, K. Inoue, M. Kurmoo, F. L. Pratt and D. Zhu, *Inorg. Chem.*, 2006, **45**, 3275; B. Zhang, Y. Zhang, Z. Gao, G. Chang, S. Su, D. Wang, Y. Guo and D. Zhu, *Eur. J. Inorg. Chem.*, 2014, 4028; B. Zhang, Y. Zhang, Z. Wang, D. Yang, Z. Gao, D. Wang, Y. Guo, D. Zhu and T. Mori, *Dalton Trans.*, 2016, **45**, 16561.

22 T. Mori, *Chem. Rev.*, 2004, **104**, 4947; N. Takubo, N. Tajima, H. Yamamoto, H. Cui and R. Kato, *Phy. Rev. Lett.*, 2013, **110**, 227401.

23 T. Mori, A. Kobayashi, Y. Sasaki, H. Kobayashi, G. Saito and H. Inokuchi, *Bull. Chem. Soc. Jpn.*, 1984, **57**, 627.

24 B. Rothaemel, L. Forro, J. R. Cooper, J. S. Schilling, M. Weger, P. Bele, H. Brunner, D. Schweitzer and H. J. Keller, *Phys. Rev. B: Condens. Matter Mater. Phys.*, 1986, **34**, 704; A. Miyazaki, T. Enoki, H. Uekusa, Y. Ohashi and G. Saito, *Phys. Rev. B: Condens. Matter Mater. Phys.*, 1997, **55**, 6847.

25 B. Zhang, Y. Zhang, Z. Wang, Z. Gao, D. Yang, D. Wang, Y. Guo and D. Zhu, *ChemistryOpen*, 2017, **6**, 320.

26 B. Bleaney and K. Bowers, *Proc. R. Soc. London*, 1952, **214**, 451; Y. Journaux, J. Sletten and O. Kahn, *Inorg. Chem.*, 1985, **24**, 4063; L. Soto, J. Garcia, E. Escriva, J. Legros, J. Tuchages, F. Dahan and A. Fuertes, *Inorg. Chem.*, 1989, **28**, 3378; O. Kahn, *Molecular Magnetism*, VCH Publisher, Inc., 1993, p. 104; P. Bergerat, O. Kahn, P. Legoll, M. Drillon and M. Guillot, *Inorg. Chem.*, 1994, **33**, 2049.

27 F. M. Romero, R. Ziessel, M. Bonnet, Y. Pontillon, E. Ressouche, J. Schweizer, B. Delley, A. Grand and C. Paulsen, *J. Am. Chem. Soc.*, 2000, **122**, 1298.

2852 | *J. Mater. Chem. C*, 2022, **10**, 2845–2852

This journal is © The Royal Society of Chemistry 2022